Journal of Nuclear Materials 539 (2020) 152345

Contents lists available at ScienceDirect

Journal of Nuclear Materials

journal homepage: www.elsevier.com/locate/jnucmat

First principles and molecular dynamics study of Li wetting and diffusion on W surfaces

Sen Xu [a], Xiaofeng Fan [a, *], Changzhi Gu [b], Yunfeng Shi [c], David J. Singh [d, e], Weitao Zheng [a, f]

[a] Key Laboratory of Automobile Materials (Jilin University), Ministry of Education, And College of Materials Science and Engineering, Jilin University, Changchun, 130012, China
[b] Laboratory of Microfabrication, Beijing National Laboratory for Condensed Matter Physics, Institute of Physics, Chinese Academy of Sciences, Beijing, 100190, China
[c] Department of Material Science and Engineering, Rensselaer Polytechnic Institute, Troy, NY, 12180, United States
[d] Department of Physics and Astronomy, University of Missouri, Columbia, MO, 65211-7010, USA
[e] Department of Chemistry, University of Missouri, Columbia, MO, 65211, USA
[f] State Key Laboratory of Automotive Simulation and Control, Jilin University, Changchun, 130012, China

ARTICLE INFO

Article history:
Received 24 March 2020
Received in revised form
17 June 2020
Accepted 19 June 2020
Available online 24 June 2020

Keywords:
Li-W Interface
Force field of W-Li
Wettability and Li diffusion
Molecular dynamics simulation

ABSTRACT

Surface diffusion is an interesting and practically important phenomenon in many areas of chemistry and physics. One emerging problem is that of Li wetting on high-Z plasma-facing metals, especially tungsten, for application in tokamak reactors. We report construction of a Li-W binary force field to describe the interface between liquid Li and solid W. We show that this force field can simulate well the atomic processes of liquid Li diffusing across the W surface, as compared with results from first-principles calculations. We find that Li atoms have different wetting behaviors on different surfaces of W. Diffusion is the fastest on the (110) surface and the slowest on the (100) surface. Diffusion of second Li layer on the (110) surface is activated at relatively low temperatures above 262 K. In addition, the diffusion rate of single-layer Li changes with the coverage rate of Li on (110) surface. High diffusion coefficients at coverage rate of $\theta = 1/6, 1/3$ and 1 are found to be related to the 2D phase transition of Li on the (110) surface.

1. Introduction

High-Z metals, such as Mo and W, with high melting point, thermal shock resistance and corrosion resistance, are potential plasma-facing materials (PFMs) for the walls of fusion reactors and/or divertors of tokamak reactors [1]. In particular, tungsten has been adopted for divertors in fusion experimental facilities EAST and ITER [2]. However, by exposing to high-energy neutron irradiation, different kinds of defects, such as voids, and impurity clusters, are introduced in these materials and result in mechanical degradation, such as swelling and brittle fracture. Liquid Li has been proved to be a promising PFM with the significant improved performance of plasma in fusion reactors [3,4]. By comparing with other PFMs, Li with low atomic number has good compatibility with plasma and particle pumping properties. Liquid Li can be injected into the interlayer or form a free surface on the inner wall to enhance plasma performance, suppress impurity fluxes and enable the operation of tokamak reactors in low recycle regimes. In this regard, it is important to analyze the wetting of liquid Li on potential plasma-facing high-Z materials, such as W and Mo. However, experiments have shown that liquid lithium does not readily wet solid wall materials [5]. Understanding the interaction between liquid lithium and solid material is the key to improve the wetting performance.

Fiflis et al. [5] and Wang et al. [6] showed that millimeter-scale lithium droplets do not wet most solid wall materials (W, Mo, C, stainless steel, etc.) at low temperature. Especially, the wetting temperature on W is greater than 580 K and varies with the surface treatment methods. However, first-principle calculations [7,8] indicated that Li with flat configuration is more stable than islands on W and Mo surfaces at zero temperature and that vacancies have little effect on the wettability. This would mean that Li can wet the

* Corresponding author.
E-mail address: xffan@jlu.edu.cn (X. Fan).

https://doi.org/10.1016/j.jnucmat.2020.152345
0022-3115/

surface of W and Mo intrinsically. These calculations were also supported by experiments [9]. A monoatomic diffusion layer was observed on the surface of tungsten (110) at 200 K [10] and stainless steel at room temperature [9]. It is important and necessary to reveal the wetting mechanism in more detail. Molecular dynamics (MD) simulation is an important method for this. In recent years, some MDs models have been proposed in an attempt to understand the microscopic wetting mechanism [11–14]. Sun et al. [11] used the Li droplet model to show that Li atoms tend to cluster on tungsten surfaces and do not wet at 500 K. On the other hand, Vella et al. [12] suggested that liquid Li can perfectly wet the surface of Mo. It is to be noted that MD simulations depend on the force fields. Establishing force fields that provide reliable atomic interactions is the key to simulate the wetting behavior. However, most of the existing multi-metal force fields are constructed to describe alloys, and few models are focused on the atomic interactions at interface. This is of particular significance for tungsten, which has a large miscibility gap and no compounds in its phase diagram with lithium.

Here, we constructed the force fields of the Li-W binary system to describe the interface interactions. These are in the framework of embedded-atom method potentials. The parameters in the force fields were fitted using results from first principles calculations by the force matching method. In the fitting, a series of characteristics, such as cohesive energy, bonding energy and diffusion barrier, are calibrated by DFT calculations. MD simulations were then performed to reveal the diffusion behaviors of liquid lithium on the surfaces of solid W. We systematically analyzed the effects of temperature, the particular W surface (i.e. the surface plane) and Li coverage on diffusion. We confirm that the Li droplet can wet the W surface. It is found that the diffusion rate of lithium between different surfaces of the substrate and also with the number of lithium layers is different. The diffusion of first Li layer is the fastest on (110) surface. The diffusion coefficient can vary by several orders of magnitude with different lithium coverage on (110) surface.

2. Computational methods and models

2.1. Details of classical molecular dynamical simulation and first principles calculations

The large-scale atomic/molecular massively parallel simulator (LAMMPS) was used to perform the MD simulations reported here [15]. The interactions between atoms were considered in the frame of embedded-atom method (see below). The simulations were performed in the NVT ensemble (conservation of particle numbers, volume and temperature) with a time step of 1 fs. The temperature was controlled by Nose-Hoover thermostats [16,17]. The atomistic configurations were visualized by the structure identification software OVITO [18].

The first principles calculations were performed on the basis of density functional theory (DFT) [19]. Projector augmented wave pseudopotentials [20] with the generalized gradient approximation (GGA) of Perdew, Burke and Ernzerhof (PBE) [21] were used in VASP code [22,23]. The plane-wave basis sets were chosen to ensure that the total energy was converged at the 1 meV/atom level. We used *k*-point meshes with a spacing of 0.02 $Å^{-1}$ to sample Brillouin zone and a plane wave expansion kinetic energy cutoff of 600 eV. For the diffusion of Li on the surface of W at dilute limit, the Nudged elastic band (NEB) calculations was used to determine the energy barriers and configurations in the transition states for the investigation of Li diffusion in the dilute limit [24].

2.2. Potential of bulk Li and W surface

We require a force field that can describe both solid and liquid phase of Li. In the processes of fitting the embedded-atom method (EAM) potential of Li-W, the interaction of Li-Li is included. In order to obtain an appropriate Li potential for solid and liquid phase of Li, the structure library in fitting the potential of lithium contains 24 structures of Li with a temperature range across the melting point (the details in SI). The effective potentials of Li with bcc structure is depicted in Fig. 1a. It shows a weak attraction and relatively flat potential curve. This reflects the low cohesive energy and modulus of Li.

Table 1 provides some properties of solid bcc Li solid from the fitted EAM potential, such as lattice constants, bulk modulus, elastic constants, cohesive energy, melting temperature and surface energies of (100), (110) and (111) surfaces. We also list the values of these parameters from experiments [25], DFT calculations and other force field predictions for the comparation [26,27]. The results obtained from our EAM potential are close to the experimental results and DFT calculations. It means the potential describes solid lithium well. Fig. 1b shows the radial distribution function curves of liquid Li from our EAM potential and X-ray diffraction [28] at 16 K above the melting point. As seen, there is a good agreement between the calculation and experiment. The melting point predicted by EAM potential is 478 K which is higher than but close to the experiment value (454K).

Here solid W is used as the substrate for the deposition and

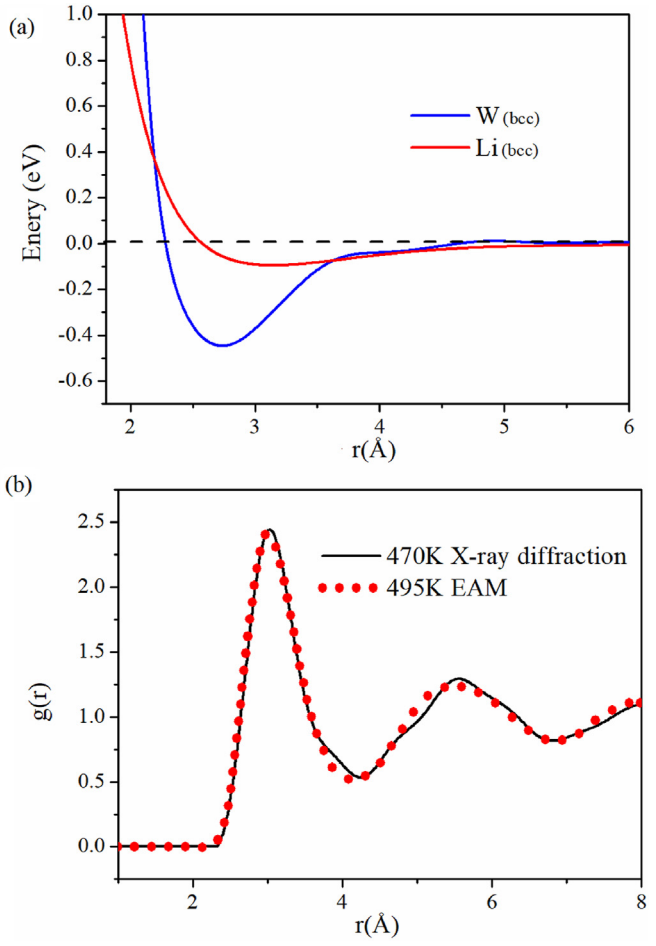

Fig. 1. (a) The effective potential for W and Li in body-centered cubic lattice, and (b) radial distribution functions of liquid Li. In (b), the melting point predicted in our EAM potential is about 25K higher than the experimental result. We choose the same temperature relative to the melting point for comparison. X-ray diffraction data are from Refs. [28].

Table 1
The lattice constants R_0, cohesive energy E_c, bulk modulus B, elastic constants, surface energies of (100), (110) and (111) surfaces, and melting temperature T_m for bulk Li from our force field. The DFT calculation and experimental results are shown when available. Values predicted by previous force fields (MEAM and 2NN-MEAM) are also listed as reference.

Li	MEAM[a]	2NN-MEAM[b]	DFT	EXP.[c]	this work (EAM)
R_0 (Å)	3.51	3.49	3.43	3.51(293K)	3.44
E_c(eV)	1.65	1.65	1.61	1.68	1.61
B (GPa)	–	13.3	14.1	–	13.7
C_{11} (GPa)	13.4	15.7	15.8	13.4	11.7
C_{12} (GPa)	11.3	12.1	13.3	11.3	14.7
C_{44} (GPa)	9.6	10.3	10.9	9.6	12.4
γ(100)(J/m^2)	0.54	0.39	0.45	0.47[d]	0.38
γ(110)(J/m^2)	0.29	0.39	0.48		0.38
γ(111)(J/m^2)	0.46	0.45	0.54		0.44
T_m (K)	–	418	–	454	478

Refs. a [26], b [27], c [25], d [37].

diffusion of liquid/solid Li. Thus, we are more concerned with the properties of the surface atoms than the internal atoms of bulk. Thus, the structural library for W-W interaction is with 27 components, including the structures with three low index face of (100), (110), and (111) was built (Details in SI). First principles calculations were performed and the results were used to fit the EAM potential for W. The resulting W potential is shown in Fig. 1a. The average atomic energies on surfaces predicted by our EAM potential are coincident with the calculated values from DFT, as shown in Table 2. The surface energies is consistent with the experimental result. It is noticed that the cohesive energy is slightly higher than DFT and experimental value [29]. Thus, the surface energies are corrected by considering the deviation of interior atoms' cohesive energies. The deviation of cohesive energy from experimental value is likely a consequence of our choice to focus on surface structures of W for the fitting. It also results in that the W-W interaction in our Li-W EAM potential doesn't describe the mechanical properties, such as elastic constants and radiation defects which is important for the search of lattice damage defects caused by the neutron irradiation. This is the shortcoming of Li-W EAM potential obtained here. Fortunately, in this work, W is just used as a solid substrate and is not directly subjected to mechanical stress during the simulation. We focus on the surfaces of W for Li diffusion. Considering the fact that temperatures (no more than 600K) that we study here are much smaller than the melting point of tungsten, internal W atom migration is negligible, and it is not expected that this difference in W cohesive energy will be important for the results.

Table 2
The lattice constants R_0, cohesive energy E_c, atomic energies on free (100), (110) and (111) surfaces (E_{sur}(100), E_{sur}(110) and E_{sur}(111)), and surface energies of (100), (110) and (111) surfaces from our W force field, DFT results, other potential and available experimental results.

W	EAM[a]	EXP	DFT	this work (EAM)
R_0 (Å)	3.17	3.17[b]	3.17	3.20
E_c (eV/atom)	−8.90	−8.90[b]	−8.91	−8.12
E_{sur}(100) (eV/atom)	–	–	−6.42	−7.18
E_{sur}(110) (eV/atom)	–	–	−7.41	−7.43
E_{sur}(111) (eV/atom)	–	–	−4.92	−4.47
γ(100) (J/m^2)	2.72	3.25[c]	3.96	3.61
γ(110) (J/m^2)	2.31	3.68[d]	3.38	3.45
γ(111) (J/m^2)	2.96		3.68	3.59

Refs. a [38], b [29], c [39], d [40].

2.3. Force field development of Li-W interaction

The Li-W potential is the key to describing the wetting behavior, since wetting involves a balance between interfacial and free surface energies. The cohesive energy is expressed with a pairwise potential and a many-body embedding energy in the EAM framework. Here, we construct the W-Li force field for study of the interface. The total energy E_i of atom i is expressed in the following form,

$$E_i = \frac{1}{2}\sum_{j\neq i}\Phi(r_{ij}) + F(n_i), \text{with } n_i = \sum_{j\neq i}\rho(r_{ij}) \quad (1)$$

where $\Phi(r_{ij})$is the pair potential which can be seen as the electrostatic repulsion between the core of atom i and that of j, and $F(n_i)$is the energy of ion core embedded in the local electron density n_i. The local electron density $n_i$is the superposition of $\rho(r_{ij})$which is contributed by the neighbor atoms.

The pair potential part is in the form of Morse potential,

$$\Phi(r) = D_e\left([1-\exp(-a(r-r_e))]^2 - 1\right)\psi\left(\frac{r-r_c}{h}\right) \quad (2)$$

The electron density function is defined as [30],

$$\rho(r) = \frac{1 + a_1\cos(\alpha r + j)}{r^\beta}\psi\left(\frac{r-r_c}{h}\right) \quad (3)$$

The embedding function is given by Ref. [31],

$$F(n) = F_0[1 - \gamma\ln(n)]n^\gamma + F_1 n \quad (4)$$

Here,$\psi(x)$is a smooth function defined as,

$$\psi(x) = \begin{cases} \dfrac{x^4}{1+x^4}, & x<0 \\ 0, & x>0 \end{cases}, \text{and}, x = \frac{r-r_c}{h} \quad (5)$$

It makes the functions $\Phi(r)$ and $\rho(r)$ smoothly approach zero at the cutoff distance. A global cutoff radius $r_c = 8$ Å is adopted. The parameter h is used to adjust the rate at which the function value drops to zero. Each of the parameters D_e, a, r_e, h, a_1, α, β, ϕ, F_0, γ and F_1 in the above, has three values corresponding to pairs of Li-Li atoms, W-W atoms and Li-W atoms, in Li-W system, respectively. In the fitting, the parameter values for Li-Li and W-W are fixed to the values for bulk Li and W surface as obtained above. We then use a structure library with 32 structures corresponding to Li adsorption on various W surfaces in different concentrations to fit the Li-W parameters. The sizes of all these structure models in the library are large enough that the lengths in all the directions are greater than the cutoff radius. We include the structures of Li-adsorbed W surfaces with low and high concentration of Li (See Fig. S1 in SI). The values of the parameters obtained are listed in Table S1-S3 of SI. The properties of these structures are calculated by first principles methods. The force matching method from potfit [32] package is used to fit the parameters to the results from first principles calculations, including the total energy and local stress for each structure.

In order to test the EAM potential, we compare the diffusion properties of single lithium atoms on W surfaces from DFT and the EAM potential. As shown in Fig. 2a, our EAM potential can predict accurately the adsorption and desorption of Li atoms on the W (110) surface. Both the energy value and curvature near the equilibrium point in the desorption curve are fitted well. As shown in Fig. 2b–d, the horizontal diffusion barriers for three low index surfaces specifically, (100), (110) and (111), are different from the DFT results only by a maximum of 14%. This difference is small, when compared

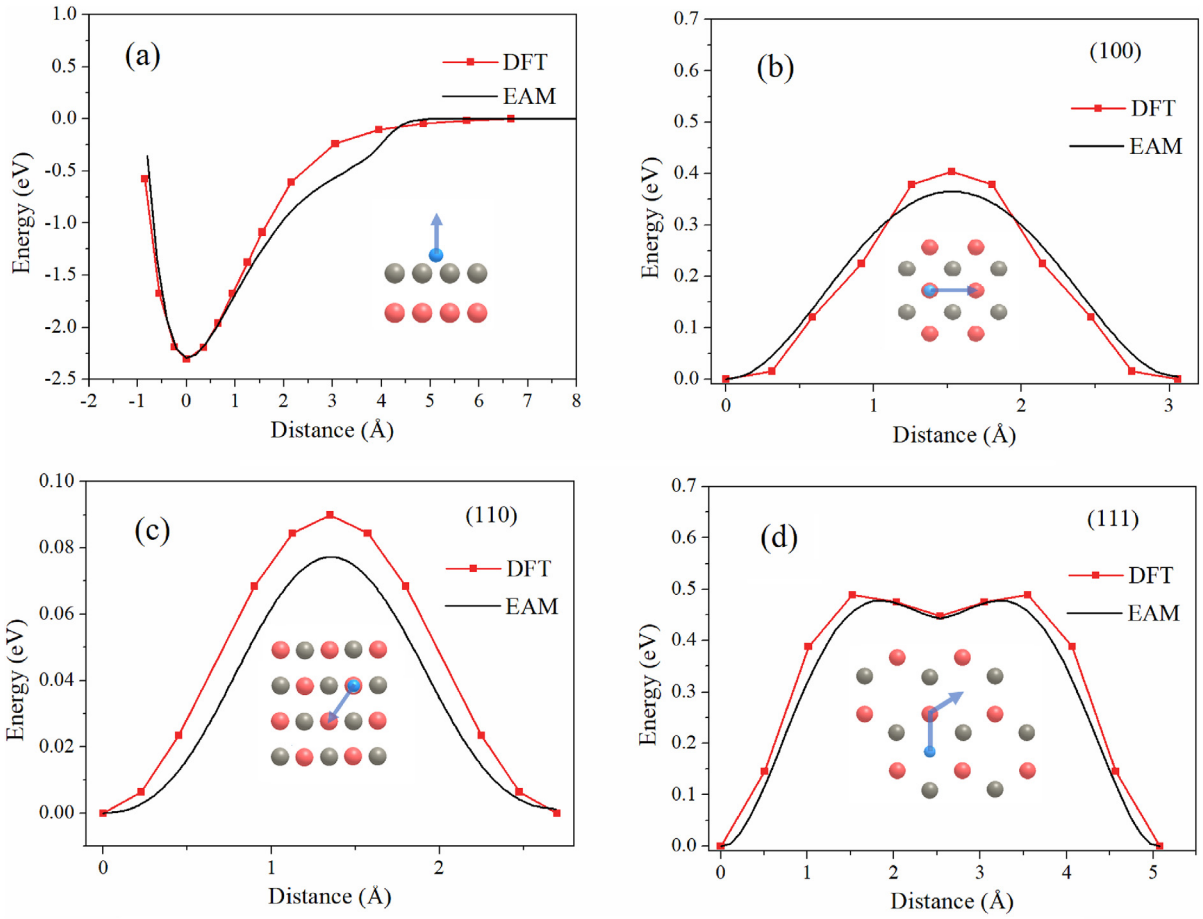

Fig. 2. The desorption curve of Li (a) and diffusion energy curve of Li diffusing in (b) the (100), (c) (110) and (d) (111) surfaces of W from MD simulation with our force field for the Li-W interface (EAM) and DFT calculations. (In the inset, the diffusion paths are shown).

with the high adsorption energy.

3. Results and discussion

3.1. Droplet of Li on different W surfaces

We now discuss the wetting behavior of fluid Li on the surface of W. We simulated the diffusion of a lithium droplet on the surface of W, including the (100), (110) and (111) surfaces. The Li droplet contains 3010 atoms with a radius of 25 Å. The thickness of the W slab in *z* direction is more than 12 atomic layers. The lengths of the slab in *x* and *y* directions are 18.5 nm, with periodic boundary conditions. The *z* direction uses a fixed boundary with a vacuum layer of 10 nm. The W slabs are relaxed at 500 K, while the six atomic layers at the bottom are fixed. Then the Li droplet is put on the surface of W slab and the Li/W slab system run at 500 K for 1000 ps to check the interaction between Li atom and W surface.

As shown in Fig. 3, a thin film of lithium is formed around the droplet due to the diffusion of Li atoms on the surface of W. The configurations indicate that Li atoms tend to occupy lattice sites on W surface and that the Li film formed reproduces the structure of W surface. A noteworthy phenomenon in the diffusion structure is that the diffusion structure has a layered characteristic. This reflects Li-W interactions. The lithium on the (110) surface expands with a single atomic layer (Fig. 3a). This phenomenon has been observed in experiments [10] and is analyzed in terms of a surface model in the next part.

Lithium on the (100) surface forms a large number of atomic layers with sharp contour boundaries (Fig. 3b). The film formed on the (111) surface consists of an atomic double layer (Fig. 3c). Starting from Fick's law, the concentration gradient from the droplet can drive the diffusion of Li atoms. There is also another mechanism that drives the film spread. It is known that the lattice constant of Li (3.51 Å) is larger than that of W (3.17 Å). This means that the adsorbed lithium atoms are highly compressed on the close packed plane. The repulsive force may be another power to drive the formation of Li film [33]. Finally, there is the attraction between Li and W which favors wetting, i.e. spread of the Li, if it is strong enough compared with the surface energy of Li (the surface tension). It is important, however, to note that a strong interaction between Li and the W surface while favoring spreading, may not lead to fast of Li atoms in contact with the W, since a strong interaction may also lead to high diffusion barriers.

We calculated the variation of the diffusion radius of Li film on different surfaces with time as depicted in Fig. 4a. The (110) surface of the bcc crystal has the highest atomic density and thus the most adsorption sites, which could be occupied by Li atoms. In addition, based on the DFT calculations, Li has a shorter diffusion path and lower diffusion barrier from one adsorption site to another on the (110) surface, as compared to the (100) and (111) surfaces. Thus, it can be expected to have the fastest diffusion rate. Actually, the droplet diffuses into a single atomic layer with a radius of 8.2 nm within about 72 ps. Transient structures in the diffusion processes are shown in Fig. 4b–d. The two-dimensional density of adsorption sites on (110) surface is $(2/(\sqrt{2}a^2)$ (a is the lattice constant of W). By comparison, the density on the (100) surface is $1/a^2$. The lower

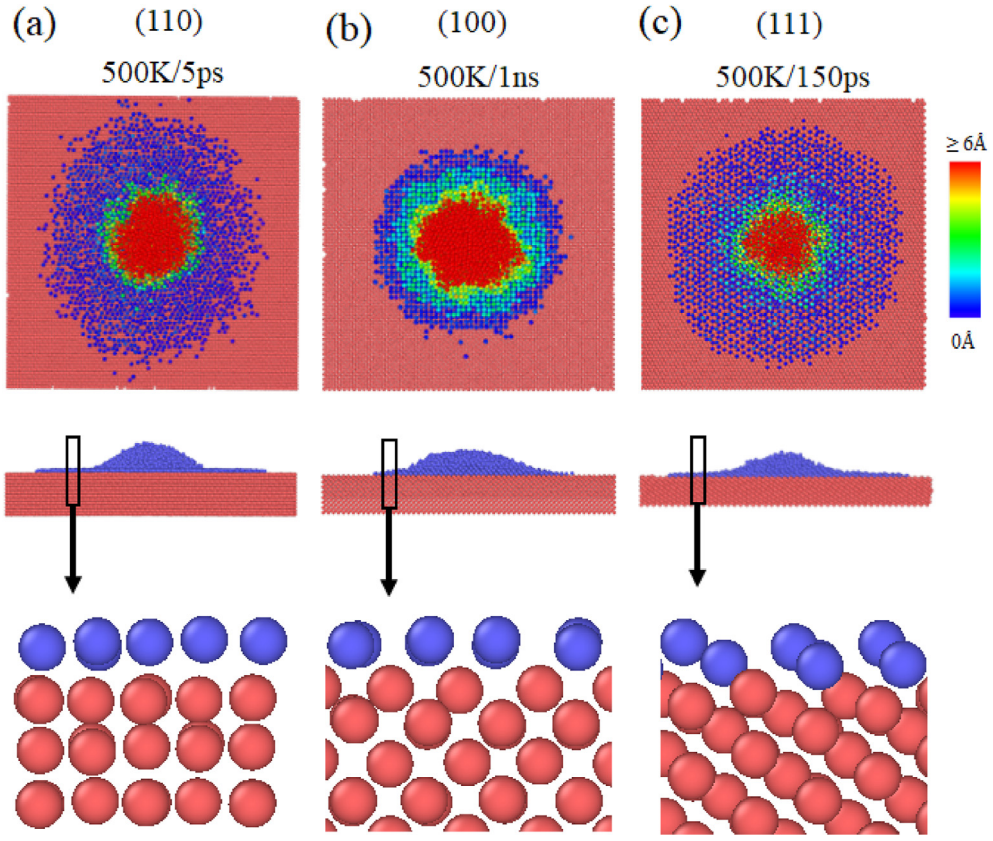

Fig. 3. Snapshots of Li droplet spread on W surfaces at 500K including (a) on the (110) surface at 5ps, (b) on the (100) surface at 1 ns and (c) on the (111) surface at 150ps. The top image is a top view and the Li atoms are colored by height. The middle is a side view and the bottom is a cross-section depicting the vertical distribution of atoms. Li and W atoms are colored in blue and red, respectively. (For interpretation of the references to color in this figure legend, the reader is referred to the Web version of this article.)

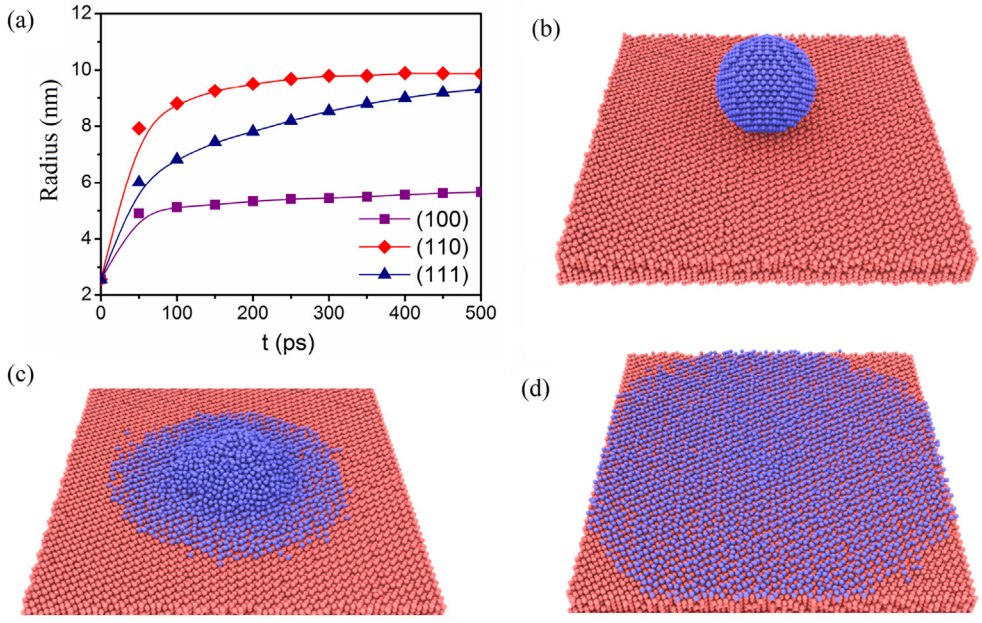

Fig. 4. (a) Curves of the extension radius of liquid lithium film on different surfaces with time due to Li diffusion on W surface at 500 K, and morphology of lithium droplets at (a) 0 ps, (b) 100 ps and 500 ps on the (110) surface of W at 500K.

density of adsorption sites and higher diffusion barrier make Li diffusion more difficult on (100) surface. Following the relatively fast diffusion at the beginning (less than 72 ps) due to the wetting of droplet and high concentration gradient of Li (with a diffusion radius of 4.9 nm in Fig. 4), the diffusion on this surface is slow. Following an initial period (72 ps), the diffusion radius just increases 0.7 nm over 430 ps. The (111) surface also has a rather low density of stable adsorption sites, $1/(\sqrt{3}a^2)$. However, there is

another set of metastable adsorption sites (Fig. 2d). These two different sites are at approximately the same height, and thus they can both participate in forming a quasi-two-dimensional Li layer through diffusion. The overall density of both sites is $2/(\sqrt{3}a^2)$. This is intermediate between the site densities of the (110) and (100) planes. Thus, the diffusion on the (111) is found to be faster than that on the (100) surface, though the diffusion barrier on the (111) surface is a little higher than that on the (100) surface. In any case, it is slow compared to diffusion on the (110) surface.

3.2. One-dimensional diffusion of Li atoms on surfaces of W

We simplify to a strip, one-dimensional model for analyzing the diffusion of Li on the surface in detail. As shown Fig. 5a, we use a simulation geometry with a rectangular W slab in *x*-*y* plane with a length of 40 nm and a width of 6 nm under periodic boundary conditions. In *z* direction, there are more than 12 atomic layers with a vacuum layer of 15 nm. A nanoribbon of Li with seven atomic layers with the periodic boundary along *y* direction is put on surface of W, and Li atoms from this nanoribbon diffuse along the *x* direction. For the (110) and (100) surface of W, the [100] direction is chosen as the diffusion direction, and for (111) face, the $[11\bar{2}]$ direction is selected. Note that while this is a one-dimensional geometry, the strip is wide enough that atoms can pass by each other, in contrast to models of diffusion on one-dimensional chains.

The system is set to 500 K to check the diffusion of Li. Fig. 5b shows the boundary of Li film on (110) surface as it changes with diffusion time. Here, a coverage of 1.0 means that the Li concentration is the same as the atomic layer density of W surface and all the stable adsorption sites are occupied. The result is similar to the observation in the simulation of Li droplets and the first diffusion layer diffuses quickly. We also observed the step of second Li layer, though it moves slowly. In addition, the boundary of the third and above atomic layers moves back, and the atoms from these layers are integrated into an island under the simulation conditions. This is mainly due to the underlying lattice mismatch, weaker adsorption force of the upper layer and surface tension of liquid Li. The layered structure can also be seen in the diffusion processes on the (100) and (111) surface (Fig. S2a of SI). For the (100) surface, which is the slowest for the Li diffusion among three surfaces in Fig. 5c, we do not find the clear steps of first layer and second layer. The island is formed from the upper layers and it has a step for the third layer of Li. For the (111) surface, the double layer of Li is formed and diffuses quickly like in the simulation of droplet, compared to that on (100) surface. But there is no clear step between double layer and other upper layers (Fig. S2b of SI). The atoms above the fourth layer aggregate to form an island. Thus, in these 1D diffusion models, we observed the formation of a liquid island in the diffusion direction, besides the initial wetting behavior and diffusion on the surface at 500 K.

The single layer of Li can be formed very quickly on the (110) surface at temperatures above melting point of Li. This indicates that the (110) surface could have excellent wetting. Then we test the diffusion of second Li layer and the effect of temperature. We repeat the simulation on the (110) surface with a lithium coverage of 1.0 (Fig. 6a). Similar to the diffusion of first layer, the diffusion step of second layer is clear (Fig. 6b). But the diffusion rate is much lower than that of first layer in Fig. 6c. The effect of temperature on diffusion is considered by analyzing the diffusion at 300 K, 500 K and 600 K. As one might expect, the diffusion rate very clearly increases with temperature as shown in Fig. 6c. Room temperature (300K) is well below the melting point of bulk Li. Even so, we still observed the boundary of first Li layer moves outward quickly. We do not observe the formation of Li island due to the low temperature (Fig. S3 of SI). The second Li layer is blocked with very slow diffusion rate even if the surface is completely covered by lithium atoms. This means more thermal energy is needed to active the second Li layer, as the diffusion at 600 K shown in Fig. 6c. We simulated the activation in detail by increasing the temperature. As shown in Fig. S4 of SI, the critical temperature to active the diffusion of second Li layer is 262 K, which is consistent with the experimental report of 250−325 K [10].

3.3. Estimating diffusion coefficient of Li on (110) surface of W

We estimate the diffusion coefficient of Li through the shape of

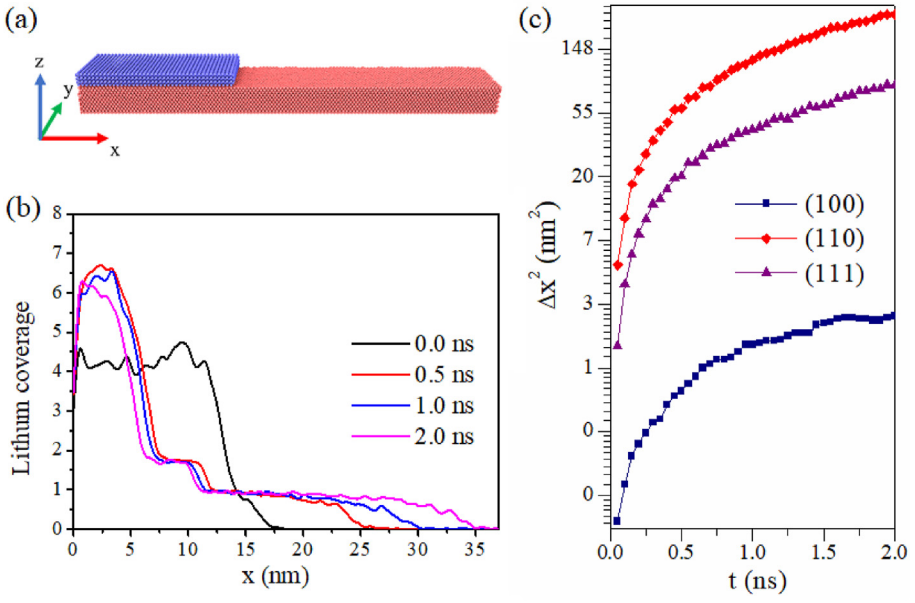

Fig. 5. (a) Schematic of one-dimensional diffusion model of Li on W surface, (b) profile changes of Li coverage over time on the W (110) surface at 500K, and (c) plots of the square of diffusion length (Δx^2) along *x* direction versus the time (*t*) on different surfaces.

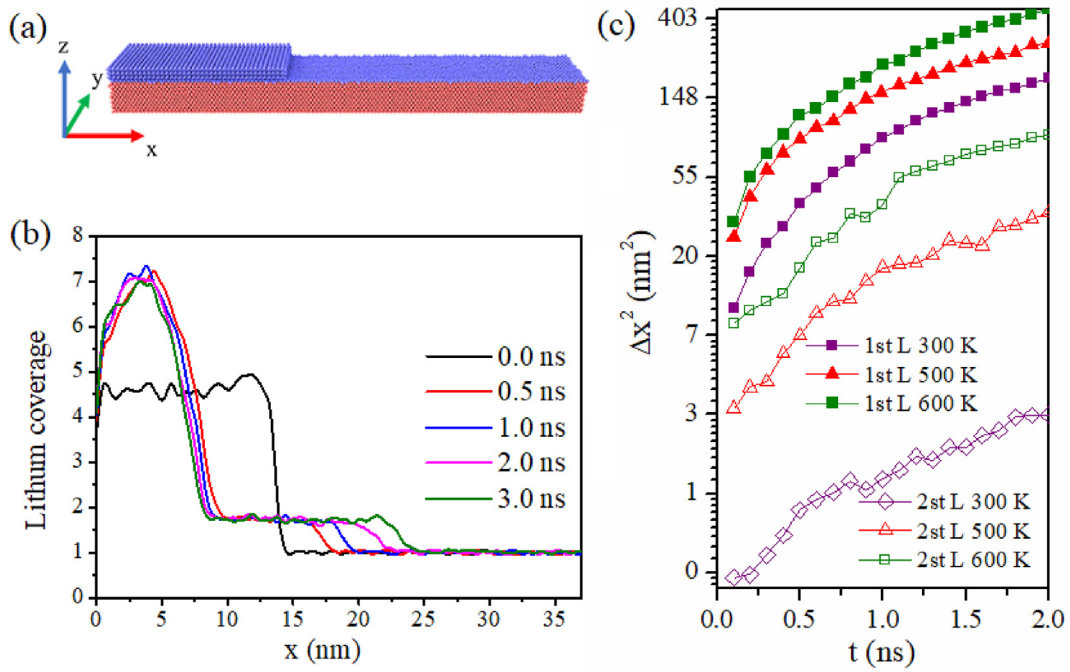

Fig. 6. (a) Initial state of second Li layer diffusion on (110) surface, (b) profile changes of Li coverage over time on the (110) surface at 500K after W (110) surface is covered fully by first Li layer, and (c) plots of the square of diffusion length (Δx^2) along x direction versus the time (t) for the first and the second Li layer on (110) surface at 300K, 500K and 600K.

diffusion plots using the formula,

$$\int_{\mu_1}^{\mu_2}(\theta-\theta_0)dx = Dt\left[\left(\frac{d\theta}{dx}\right)_{\mu_1}-\left(\frac{d\theta}{dx}\right)_{\mu_2}\right] \quad (6)$$

where μ_1 andμ_2 are the coordinates in the diffusion direction x, $\theta_0$and $\theta$are the values of coverage at a given x before and after diffusion for a period of time, respectively. D is the diffusion coefficient and t is the diffusion time. We constructed two models with two different initial coverages (θ_0) of single layer Li nanoribbon to eliminate the effect of the initial configuration on the results. The first model has one step for the Li nanoribbon on (110) surface of W, and another one has continuous concentration gradient, as shown in Fig. 7a and Fig. S5 of SI. We did simulations at 300 K and 500 K.

The results are shown in Fig. 7b and the diffusion coefficient is not correlated to the initial configuration of Li nanoribbon. It is clear that diffusion coefficient increases with the temperature as is normal. It is also observed that diffusion coefficient is dependent on the coverage rate of Li. In the very low coverage of Li (dilute limit), atomic thermal motion on surface behaves like two-dimensional Brownian motion. We examined the thermal motion of single Li atoms at 300 K and 500 K and diffusion coefficient is calculated by using Einstein diffusion model with the formula,

$$D = \lim_{t\to\infty}\frac{<x^2>}{2t} \quad (7)$$

where $<x^2>$ is the mean-squared displacement in [100] direction and t is the diffusion time. We averaged the data from 100 isolated atoms for 1 ns. The results are labeled with stars in Fig. 7b, and they fit well with the values of D at the limit of zero coverage. We can plot the change of D following the increase of temperature with the formula, $D = D_0\exp(-E_d/K_BT)$, where E_d is the activation energy and D_0 is the preexponential factor. E_d is approximately equal to the diffusion barrier from first principles calculations. By fitting the parameter D_0, the curve of D is plotted in Fig. 8a. It is consistent with the experimentally reported values from 100 K to 200 K [10].

Available experimental data for high coverage at low temperatures, as labeled with black and red squares, are shown in Fig. 7b. The simulation results are consistent with the experiments with high coverage, while the diffusion coefficient from MD is a little higher at the coverage rate of 0.7–0.9 at 300 K. This difference may be due to the fact that the coverage rate θ in simulation is calculated on the basis of the average number of a region, which may include local partial regions with high coverage rate close to 1.0. The diffusion coefficients at the coverage rate near the coverage limit of $\theta = 1$ are higher than those at θ of about 0.8 by more than two orders of magnitude at 300 K. In addition, it is also possible that the defects on surface in experimental samples can block the diffusion and thus decrease the diffusion coefficient.

We have observed that the diffusion coefficient increases with the increase of coverage rate up to $\theta = 1/3$ and then drops with the further increase of coverage. In addition, as the coverage rate close to 1.0, the diffusion coefficient has a leap with the formation of the chains of 2D vacancies (Fig. S6 of SI). Coverage rate $\theta = 1/3$ and 1 are the local maxima positions in the curve of diffusion coefficient for the simulations at 300 K and 500K. The two obvious local maxima of D in the curve are proposed to be related to the first-order phase transition of single-layer Li on (100) surface of W. For some coverage rate with the presence of phase transitions, the diffusion coefficient D is expressed as $D = \Phi D_{c.m.}$, where $D_{c.m.}$ is the center-of-mass diffusion coefficient as we well known and Φ is the thermodynamic factor [34]. Near some stable phase, the thermodynamic factor Φ increases quickly and thus result in the increase of D [35]. This is because the formation of stable phase can decrease the free energy of system and thus the formation of it can enhance thermodynamic factor and increase the value of D. Therefore, we attribute the two maxima near $\theta = 1/3$ and 1 to the formation of two new ordered phases of Li.

Indeed, there are phase transitions with a new ordered phase at $\theta = 1/3$ and 1, as seen in the experimental observation of on (110)

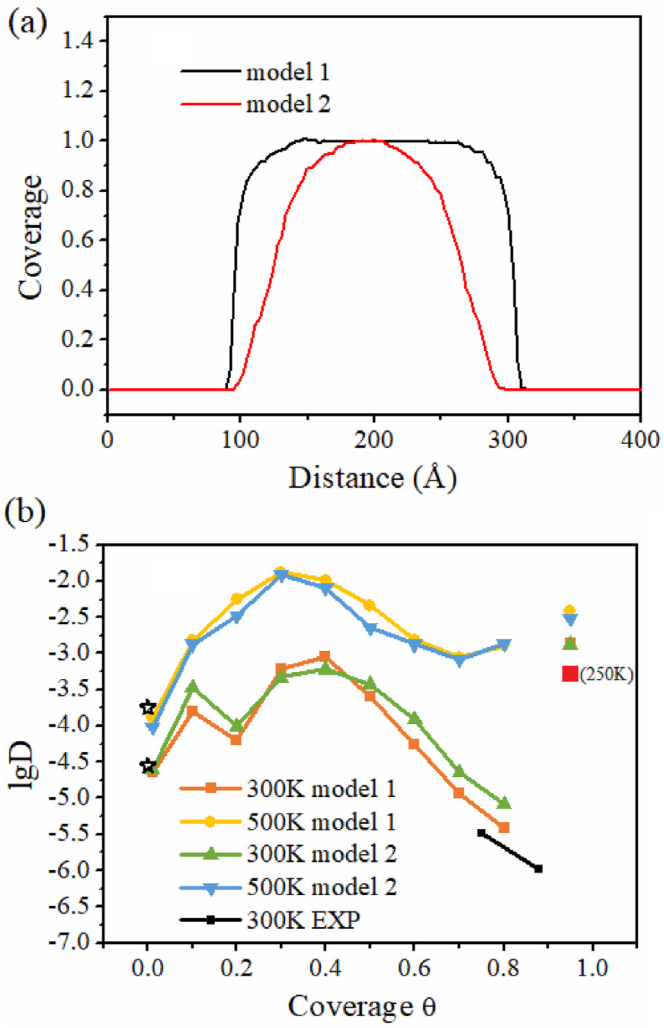

Fig. 7. (a) The initial coverage profiles of two models used in calculating the diffusion coefficient, and (b) plots of lg D versus θ (D in cm^2s^{-1}) at 300K and 500K. The star labels are results with Einstein diffusion model and the black squares and red square is from experimental values. (For interpretation of the references to color in this figure legend, the reader is referred to the Web version of this article.)

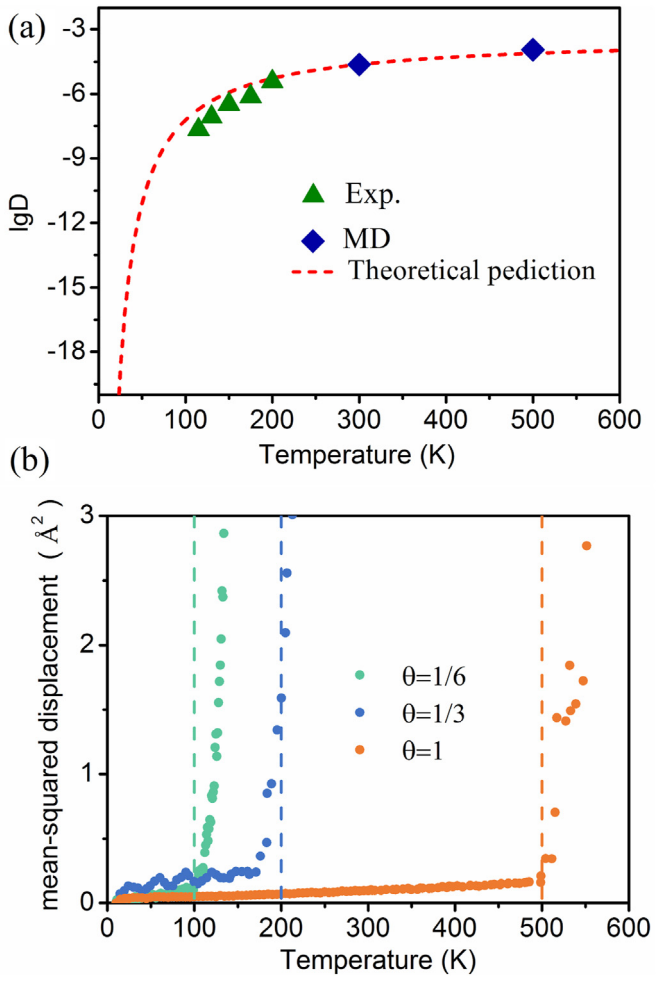

Fig. 8. (a) Plots of theoretical calculated the curve of D (D in cm^2/s) with the experimental values and values of MD simulation, and (b) mean-squared displacement for 2D Li lattice on (110) surface of W with the coverage of $\theta = 1/6$, 1/3 and 1. The dash lines are experimental temperatures of order-disorder transition.

surface of W by low-energy electron diffraction [36]. The first-order phase transitions take place at $\theta = 1/3$ and 1. The ordered phase at $\theta = 1$ is easy to understand because there is no other sites for localized diffusion of Li on 2D plane (this is full coverage). This phase is very stable and the phase transition temperature from the order to the disorder is about 500 K in our simulation and as in the experimental result as shown in Fig. 8b [10]. We also simulated the phase transition of $\theta = 1/3$ and the transition temperature is about 180 K and consistent to the observation (200 K) in experiments [36]. In addition, there is an ordered phase at $\theta = 1/6$ observed in experiment [36]. This may explain the local maximum value of D at 300 K around $\theta = 1/6$ in Fig. 7b. However, at 500 K, we do not find this local maximum value around $\theta = 1/6$. This implies that the ordered phase at $\theta = 1/6$ is not as stable and disappears at 500K. We simulate the phase transition at $\theta = 1/6$ and the transition temperature is just 100 K. Thus at high temperature the influence of this ordering on the diffusion coefficient is not seen.

3.4. Comparison with experimental results

From the simulation results, lithium droplet can wet the W substrate well (with a single Li atomic layer) at 500 K which is near the melting temperature of Li, though the diffusions of Li atoms are different in different surfaces of W, including (001), (110) and (111) surface. Actually, the wetting behavior on W surfaces is related to the interaction of Li-W in the microscopic view. With the DFT calculation, it is known that interaction between Li and W(about 2.3 eV in Fig. 2a) is stronger than the Li-Li interaction. Thus, with the contact between Li droplet and W surface, Li atoms would like to be adsorbed on W surface. Under the thermal activation and concentration gradient, Li atoms will diffuse on W surfaces to form the initial wetting from the macroscopic view, since the diffusion barriers of Li atom on W surfaces are small, as seen in Fig. 2b–d. Similar situations are also appeared on other substrates, such as stainless steel. The Li adsorption energy (2.52 eV) on the surface of unoxidized stainless steel (similar to the adsorption on W surface) is higher than Li-Li binding energy of 1.54 eV [9]. As the experimental report of Skinner et al. with the technique of temperature programmed desorption [9], in the absence of oxidation layer, lithium-stainless bonding is more energetically favorable than Li-Li bonding. Under ultrahigh vacuum condition, they observed with the scanning Auger microprobe that the lithium from mm-scale particle could actually spread on the adjacent strainless steel surfaces. In other experiments [5,6], it was observed that lithium droplets didn't wet most solid wall materials at low temperature

such as W, Mo, and stainless steel. These experiments were performed by observing the change of contact angle. For an example, at 200 °C, a contact angle of 130° for lithium droplet on W substrate was observed in the experiment of Fiflis et al. [5]. They also observed the decrease of contact angle with the temperature increase. This indicates Li from lithium droplet can wet the W surfaces at higher temperature. Fiflis et al. confirmed that Li didn't wet lithium oxide [5]. In addition, the native oxide layer is formed easily on the surface of some substrates if the experiment isn't performed under high vacuum condition. The oxygen on the surface of substrates, such as W, results easily in the formation of lithium oxide and thus introduces the kinetic barrier to block the wetting of Li and raises the wetting temperature. With the blocking of Li diffusion on the surfaces, the slow diffusion rate will make the surface tension a real role in the case of Li droplet, and thus the large contact angle is observed. As the observation of Fiflis et al. [5], glow discharge cleaning of W surface can decrease the wetting temperature. With the coating of Li thin layer on the surface of substrates to decrease the effect of oxygen and lithium oxide, Li can wet the substrate under very low temperature, less than 180 °C. This is consistent with our simulation result that the second Li layer can diffuse under the covering of first Li layer on W surfaces. For the ITER-grade-W under high vacuum environment, the oxygen effect should be weak, and thus it will be a suitable material for liquid Li.

4. Conclusions

An embedded-atom type Li-W force field is constructed to describe the interface interaction of liquid Li and solid W and thereby to explore the wetting and diffusion behaviors on the surface of W. The parameters of force field are established by fitting the results from first principles calculations with the force matching method. The important characteristics of Li and W, such as lattice constants, bulk modulus, and melting temperature of Li, surface energies of W, and so on, based on our fitted EAM force field is consistent with experimental results and other DFT calculations. The interaction between Li and W and the diffusion of single Li atoms on the surface of W are also similar to those from our DFT results. These force fields are then used in MD simulations to study atomic mechanisms of liquid Li film spreading on W surfaces. We find that Li can wet the surface of W and form layered structures when adsorbed on the surface. The (110) surface has the highest diffusion rate. The (100) surface limits the migration of Li atoms. On the (110) surface, Li atoms can diffuse at the temperatures below melting point of Li, such as room temperature. The diffusion rate of first layer Li is higher than that of second layer by about two orders of magnitude at 500 K. The diffusion rate is found to change very substantially with the coverage rate. In additional local maxima in the diffusion rate vs. coverage rate are found. They may be related to the phase transition of single-layer Li on (110) surface. It is hoped that the present results, which show complex behavior in the initial wetting of W surfaces by Li, will be useful in the understanding of the Li-W interactions and will stimulate the further experimental research on this topic.

CRediT authorship contribution statement

Sen Xu: Investigation, Software, Visualization, Writing - original draft. **Xiaofeng Fan:** Conceptualization, Methodology, Formal analysis, Investigation, Supervision, Writing - review & editing. **Changzhi Gu:** Conceptualization, Writing - review & editing. **Yunfeng Shi:** Writing - review & editing. **David J. Singh:** Formal analysis, Writing - review & editing. **Weitao Zheng:** Conceptualization, Writing - review & editing.

Declaration of competing interest

The authors declare that they have no known competing financial interests or personal relationships that could have appeared to influence the work reported in this paper.

Acknowledgments

The research was supported by the National Key R&D Program of China (Grant No. 2016YFA0200400) and the National Natural Science Foundation of China (Grant No. 51627805).

Appendix A. Supplementary data

Supplementary data related to this article can be found at https://doi.org/10.1016/j.jnucmat.2020.152345.

References

[1] J.N. Brooks, L. El-Guebaly, A. Hassanein, T. Sizyuk, Plasma-facing material alternatives to tungsten, Nucl. Fusion 55 (2015), 043002.
[2] D.M. Yao, G.N. Luo, Z.B. Zhou, L. Cao, Q. Li, W.J. Wang, L. Li, S.G. Qin, Y.L. Shi, G.H. Liu, J.G. Li, Design, R&D and commissioning of EAST tungsten divertor, Phys. Scripta T167 (2016), 014003.
[3] G.Z. Zuo, J.S. Hu, R. Maingi, Z. Sun, Q.X. Yang, M. Huang, X.C. Meng, W. Xu, Y.Z. Qian, C.L. Li, H.L. Bi, Y. Chen, X.L. Yuan, X.F. Han, X. Zhu, Y.F. Wang, L. Zhang, H.Q. Liu, L. Wang, X.Z. Gong, K. Tritz, A. Diallo, R. Lunsford, M.J. Ni, J.G. Li, Results from an improved flowing liquid lithium limiter with increased flow uniformity in high power plasmas in EAST, Nucl. Fusion 59 (2019), 016009.
[4] G.N. Guo, X.D. Zhang, D.M. Yao, X.Z. Gong, J.L. Chen, Z.S. Yang, Q. Li, B. Shi, J.G. Li, Overview of plasma-facing materials and components for EAST, Phys. Scripta T128 (2007) 1–5.
[5] P. Fiflis, A. Press, W. Xu, D. Andruczyk, D. Curreli, D.N. Ruzic, Wetting properties of liquid lithium on select fusion relevant surfaces, Fusion Eng. Des. 89 (2014) 2827–2832.
[6] J. Wang, H. Wang, J. Xie, A. Yang, A. Pei, C.L. Wu, F. Shi, Y. Liu, D. Lin, Y. Gong, Y. Cui, Fundamental study on the wetting property of liquid lithium, Energy Storage Mater. 14 (2018) 345–350.
[7] M. Chen, J. Roszell, E.V. Scoullos, C. Riplinger, B.E. Koel, E.A. Carter, Effect of temperature on the desorption of lithium from molybdenum(110) surfaces: implications for fusion reactor first wall materials, J. Phys. Chem. B 120 (2016) 6110–6119.
[8] S. Yi, G. Li, Z. Liu, W. Hu, H. Deng, First-principles calculations on the wettability of Li atoms on the (111) surfaces of W and Mo substrates, Plasma Phys. Rep. 44 (2018) 692–701.
[9] C.H. Skinner, A.M. Capece, J.P. Roszell, B.E. Koel, Spreading of lithium on a stainless steel surface at room temperature, J. Nucl. Mater. 468 (2016) 26–30.
[10] A.T. Loburets, A.G. Naumovets, Y.S. Vedula, Surface diffusion of lithium on (011) face of tungsten, Surf. Sci. 120 (1982) 347–366.
[11] X. Sun, S. Xiao, H. Deng, W. Hu, Molecular dynamics simulation of wetting behaviors of Li on W surfaces, Fusion Eng. Des. 117 (2017) 188–193.
[12] J.R. Vella, M. Chen, S. Fürstenberg, F.H. Stillinger, E.A. Carter, P.G. Debenedetti, A.Z. Panagiotopoulos, Characterization of the liquid Li-solid Mo (1 1 0) interface from classical molecular dynamics for plasma-facing applications, Nucl. Fusion 57 (2017), 116036.
[13] X. Chen, X. Sun, H. Deng, S. Xiao, X. Gan, X. Li, W. Hu, The wetting properties of Li droplet on Cu surfaces: a molecular dynamics study, Comput. Mater. Sci. 119 (2016) 114–119.
[14] C. Zou, X. Sun, C. Xu, X. Li, S. Xiao, H. Deng, F. Gao, W. Hu, Wetting characteristics of lithium droplet on iron surfaces in atomic scale: a molecular dynamics simulation, Comput. Mater. Sci. 149 (2018) 435–441.
[15] S. Plimpton, Fast parallel algorithms for short-range molecular dynamics, J. Comput. Phys. 117 (1995) 1–19.
[16] S. Nosé, A unified formulation of the constant temperature molecular dynamics methods, J. Chem. Phys. 81 (1984) 511–519.
[17] W.G. Hoover, Canonical dynamics: equilibrium phase-space distributions, Phys. Rev. A 31 (1985) 1695.
[18] A. Stukowski, Visualization and analysis of atomistic simulation data with OVITO–the Open Visualization Tool, Model. Simulat. Mater. Sci. Eng. 18 (2010), 015012.
[19] P. Hohenberg, W. Kohn, Inhomogeneous electron gas, Phys. Rev. 136 (1964) B864.
[20] P.E. Blöchl, Projector augmented-wave method, Phys. Rev. B 50 (1994), 17953.
[21] J.P. Perdew, K. Burke, M. Ernzerhof, Generalized gradient approximation made simple, Phys. Rev. Lett. 77 (1996) 3865.
[22] G. Kresse, J. Furthmüller, Efficiency of ab-initio total energy calculations for metals and semiconductors using a plane-wave basis set, Comput. Mater. Sci. 6 (1996) 15–50.

[23] G. Kresse, J. Furthmüller, Efficient iterative schemes for ab initio total-energy calculations using a plane-wave basis set, Phys. Rev. B 54 (1996), 11169.
[24] G. Henkelman, B.P. Uberuaga, H. Jónsson, A climbing image nudged elastic band method for finding saddle points and minimum energy paths, J. Chem. Phys. 113 (2000) 9901–9904.
[25] C.J. Smithells, E.A. Brandes, G.B. Brook, Smithells Metals Reference Book, Butterworth-Heinemann, 1992.
[26] X.L. Yuan, K. Takahashi, Y. Yin, T. Onzawa, Development of modified embedded atom method for a bcc metal: lithium, Model. Simulat. Mater. Sci. Eng. 11 (2003) 447.
[27] Y.M. Kim, I.H. Jung, B.J. Lee, Atomistic modeling of pure Li and Mg–Li system, Model. Simulat. Mater. Sci. Eng. 20 (2012), 035005.
[28] H. Olbrich, H. Ruppersberg, S. Steeb, Experimental determination of the form and structure factor of molten lithium, Z. Naturforsch. 38 (1983) 1328–1336.
[29] E. Lassner, W.D. Schubert, Tungsten, Springer US, 1999.
[30] S. Chantasiriwan, M. Milstein, Higher-order elasticity of cubic metals in the embedded-atom method, Phys. Rev. B 53 (1996), 14080.
[31] A. Banerjea, J.R. Smith, Origins of the universal binding-energy relation, Phys. Rev. B 37 (1988) 6632.
[32] P. Brommer, A. Kiselev, D. Schopf, P. Beck, J. Roth, H.R. Trebin, Classical interaction potentials for diverse materials fromab initiodata: a review of potfit, Model. Simulat. Mater. Sci. Eng. 23 (2015), 074002.
[33] A.G. Naumovets, Collective surface diffusion: an experimentalist's view, Physica A 357 (2005) 189–215.
[34] T. Ala-Nissila, R. Ferrando, S.C. Ying, Collective and single particle diffusion on surfaces, Adv. Phys. 51 (2002) 949–1078.
[35] I. Medved, A. Trník, Collective surface diffusion near a first-order phase transition, Phys. Rev. B 83 (2011), 233406.
[36] A.G. Naumovets, A.G. Fedorus, Disordering of submonolayer films of electropositive elements adsorbed on metals, Zh. Eksp. Teor. Fiz. 73 (1977) 1085–1092.
[37] B.J. Keene, Review of data for the surface tension of pure metals, Int. Mater. Rev. 38 (1993) 157–192.
[38] M.-C. Marinica, L. Ventelon, M.R. Gilbert, L. Proville, S.L. Dudarev, J. Marian, G. Bencteux, F. Willaime, Interatomic potentials for modelling radiation defects and dislocations in tungsten, J. Phys. Condens. Matter 39 (2013), 395502.
[39] W.R. Tyson, W.A. Miller, Surface free energies of solid metals: estimation from liquid surface tension measurements, Surf. Sci. 62 (1977) 267.
[40] F. R. de Boer, R. Boom, W.C.M. Mattens, A.R. Miedema, A.K. Niessen, Cohesion in Metals: Transition Metal Alloys, North- Holland, Amsterdam, 1989.